

Leptonic Observables in Ultra-Relativistic Heavy Ion Collisions

J.L. Nagle^a for the PHENIX Collaboration*

^aColumbia University, New York, NY 10027, USA

We report on leptonic observables by the PHENIX experiment from data taken during Run II at the Relativistic Heavy Ion Collider (RHIC). We show first results on $\phi \rightarrow K^+K^-, e^+e^-$, low and intermediate mass dielectron continuum, single electrons from charm, and J/ψ yields in proton-proton and Au-Au collisions at $\sqrt{s_{NN}} = 200$ GeV.

1. PHENIX Experiment at RHIC

The PHENIX experiment was designed with the specific capability of sampling high luminosity proton-proton, proton-ion and ion-ion collisions. This feature, combined with a suite of detectors for measuring both electrons in two central arm spectrometers and muons in two forward arm spectrometers, allows for a large range of interesting measurements that probe the earliest stages of the hot quark-gluon matter created at RHIC. Further details of the detector design and performance are given in [1].

The PHENIX experiment consists of two central spectrometer arms that were completely instrumented in Run II at RHIC. The central arms each cover pseudorapidity ($|\eta| < 0.35$), transverse momentum ($p_T > 0.2$ GeV/c), and 90 degrees in azimuthal angle ϕ . They are comprised from the inner radius outward of a Multiplicity and Vertex Detector (MVD), Drift Chambers (DC), Pixel Pad Chambers (PC), Ring Imaging Cherenkov Counter (RICH), Time Expansion Chamber (TEC), Time-of-Flight Scintillator Wall (TOF), and two types of Electromagnetic Calorimeters (EMC). This combination of detectors is necessary for the clean identification of electrons over a broad range in transverse momentum. In addition, we have excellent photon capabilities with the EMC and high precision hadron identification with our smaller coverage TOF system.

PHENIX has two forward muon spectrometers consisting of hadronic absorbers, a cathode strip chamber muon tracking system, and interleaved Iarocci tubes with steel plates for muon identification and triggering. Each spectrometer covers approximately $1.2 < |\eta| < 2.2$ and $p_{tot} > 2$ GeV/c. The south muon spectrometer was commissioned and operational in Run II, while the north arm is currently being completed and will be ready for data taking in Run III.

Au-Au and proton-proton collisions are characterized with minimum bias triggers based on a set of zero degree calorimeters (ZDC), beam-beam counters (BBC), and a scintillator multiplicity counter (NTC) for larger coverage in proton-proton collisions.

*for the full PHENIX Collaboration author list and acknowledgements, see Appendix "Collaborations" of this volume.

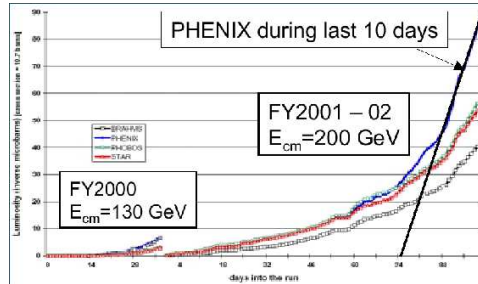


Figure 1. Integrated Au-Au luminosity delivered by the RHIC accelerator to each of the four experimental intersection regions as a function of days into the run.

2. Run II at RHIC

During the second running period at RHIC the accelerator achieved full design energy $\sqrt{s_{NN}} = 200$ GeV for Au-Au collisions. RHIC delivered to the PHENIX intersection region approximately $42 \mu\text{b}^{-1}$ within a vertex z range ($|z| < 45$ cm). PHENIX was successful in sampling this luminosity with a combination of “minimum bias” triggers and a full complement of software based Level-2 triggers. As shown in Figure 1, over 50% of the integrated luminosity was delivered during the last two weeks of the Au-Au running period. Thus, we are seeing just the beginning of high luminosity running at RHIC. In the analysis shown in these proceedings, we have scanned of order 26 million “minimum bias” events with $|z| < 30$ cm.

The RHIC accelerator also commissioned polarized proton-proton collisions and had five weeks of experiment data taking. The collisions were at $\sqrt{s} = 200$ GeV for optimal comparison with the Au-Au data set. The PHENIX experiment commissioned a first set of fully pipelined hardware Level-1 triggers including triggers on high energy photons, single electrons, single muons, and dielectrons and dimuons from J/ψ . We observed with “minimum bias” and Level-1 triggers approximately 150 nb^{-1} .

3. ϕ Meson

The $\phi(1020)$ vector meson is particularly interesting because the restoration of approximate chiral symmetry at high temperature may modify the ϕ mass and width [2]. These modifications may result in a change in the branching fraction of $\phi \rightarrow K^+K^-$ and $\phi \rightarrow e^+e^-$ when the ϕ decays in medium. Note that the ϕ lifetime $\tau \approx 44 \text{ fm}/c$ is longer than the expected lifetime of the coupled collision system, and thus only a fraction may decay in the hot fireball. It has also been hypothesized that final state interactions of kaons from ϕ decay may lower the apparent measured branching fraction in the kaon channel [3]. PHENIX has the unique ability to reconstruct the ϕ meson in both the K^+K^- and e^+e^- channels.

PHENIX has excellent kaon particle identification using our high precision time-of-flight scintillator wall. Shown in Figure 2 is the K^+K^- invariant mass distribution after mixed

event background subtraction. The distribution is for minimum bias (0-90% central) Au-Au collisions at $\sqrt{s_{NN}} = 200$ GeV. The signal to background ratio is 1/12 and the mass peak and width values agree within errors with the Particle Data Group values. More details are shown in [4]. After correcting for acceptance, efficiencies, and the branching fraction in vacuum $\phi \rightarrow K^+K^-$ (0.49), we find:

$$\phi \text{ (via } K^+K^-) : \left. \frac{dN}{dy} \right|_{y=0} = 2.01 \pm 0.22(\text{stat})_{-0.52}^{+1.01}(\text{sys}) \quad [\text{PRELIMINARY}] \quad (1)$$

This value is in agreement with the STAR experiment results reported at this conference [5] within errors. We have higher statistics using time information from our larger coverage electromagnetic calorimeter for particle identification. We expect to have transverse mass distributions for a full range of Au-Au centrality bins shortly.

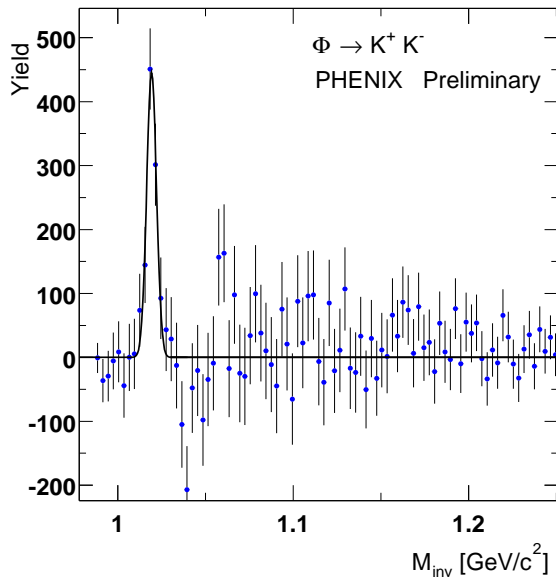


Figure 2. K^+K^- invariant mass distribution after mixed event subtraction for minimum bias (0-90% central) Au-Au collisions at $\sqrt{s_{NN}} = 200$ GeV.

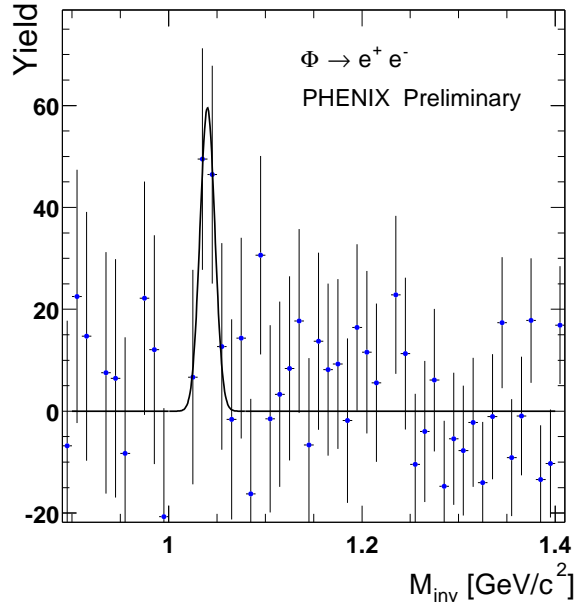


Figure 3. e^+e^- invariant mass distribution after mixed event subtraction for minimum bias (0-90% central) Au-Au collisions at $\sqrt{s_{NN}} = 200$ GeV.

PHENIX has excellent electron identification capabilities that are necessary to separate electrons from the much more abundant charged pions. The RICH yields a threshold selection for electrons, the TEC allows for pion-electron separation at low momentum due to different energy loss dE/dx , and the EMC is used to verify a tracking momentum-electromagnetic energy match. We show in Figure 3 the e^+e^- invariant mass distribution

after mixed event background subtraction. There is an excess of counts at the ϕ mass with a signal strength of $101 \pm 47(\text{stat})_{-20}^{+56}(\text{sys})$ and a signal to background ratio of 1/20. Within relatively large errors the mass peak and width values agree with the values from the Particle Data Group. Using the signal value quoted above, we have corrected for the acceptance and efficiencies, and assuming the branching fraction in vacuum $\phi \rightarrow e^+e^- = 2.9 \times 10^{-4}$, we find:

$$\phi \text{ (via } e^+e^- \text{)} : \left. \frac{dN}{dy} \right|_{y=0} = 5.4 \pm 2.5(\text{stat})_{-2.8}^{+3.4}(\text{sys}) \quad [\text{PRELIMINARY}] \quad (2)$$

Although the electron and kaon results differ, they are consistent within 1σ statistical errors. We need further statistics in the electron channel from future running.

4. Dielectron Continuum

In the dielectron invariant mass region below the ϕ , referred to as the Low Mass Region (LMR), there may be excess dielectrons from in-medium mass modification of the ρ meson due to restoration of approximate chiral symmetry or collision broadening [6]. In the region above the ϕ and below the J/ψ , referred to as the Intermediate Mass Region (IMR), there may be a significant contribution from semi-leptonic decays of open charm D mesons at RHIC energies.

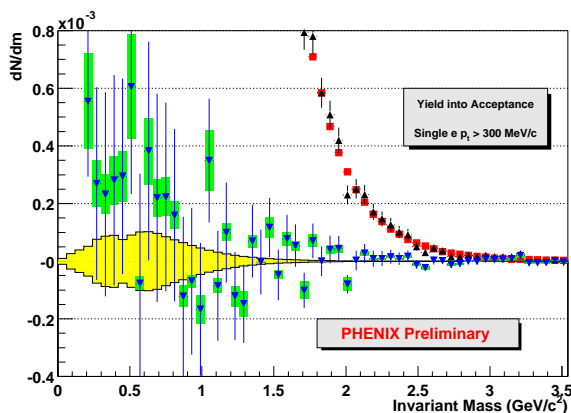


Figure 4. dN/dm (c^2/GeV) into the PHENIX acceptance in “minimum bias” Au-Au events for dielectrons as a function of invariant mass after mixed event background subtraction.

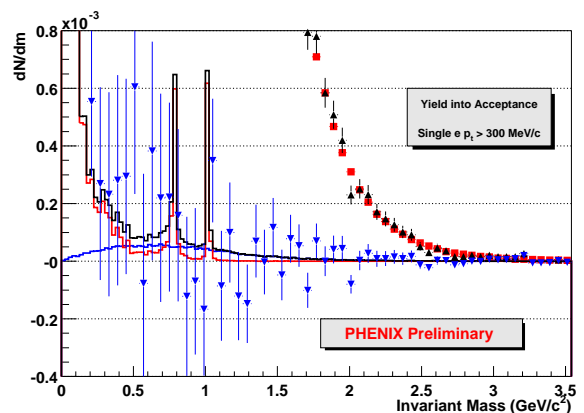


Figure 5. Same data as in left figure without systematic error bands. Data is overlaid with “baseline” expectations calculation assuming no medium modifications.

We show in Figure 4 dN/dm into the PHENIX acceptance as a function of dielectron invariant mass after mixed event background subtraction with statistical and systematic errors. Note that we have corrected for our efficiencies relative to our PHENIX specific

acceptance, and will publish our simple acceptance definition shortly. The solid band represents the systematic error in the normalization of the mixed event background, while the individual bands are the point to point systematics. We show the same distribution in Figure 5 with a simple “cocktail” model of expected baseline contributions (black), including light meson decays (red) and a PYTHIA charm calculation scaled by the number of binary collisions (blue).

In the LMR ($M_{inv} = 0.3 - 1.0 \text{ GeV}/c^2$), the dominant expected contributions are from meson Dalitz decays and low mass vector meson decays (including the ω). Assuming no medium modifications we expect a yield of $N = 9.2 \times 10^{-5}$ (counts/event). The PHENIX preliminary result is:

$$N (\text{LMR, into PHENIX}) = 13.4 \pm 7.2(\text{stat})_{-8.4}^{+12.2}(\text{sys}) \times 10^{-5} \text{ [counts/event]} \quad (3)$$

The large statistical and systematic errors prevent an observation of the ω meson or conclusions about ρ mass shifts at this time.

In the IMR ($M_{inv} = 1.1 - 2.5 \text{ GeV}/c^2$), the dominant expected contribution is from the correlated semi-leptonic decays of D and associated \bar{D} mesons. Using a PYTHIA charm calculation, assuming binary collision scaling for ion-ion reactions, we would expect $N = 1.5 \times 10^{-5}$ (counts/event). Our preliminary result in the IMR is:

$$N (\text{IMR, into PHENIX}) = 0.38 \pm 2.60(\text{stat})_{-0.81}^{+1.40}(\text{sys}) \times 10^{-5} \text{ [counts/event]} \quad (4)$$

This result is consistent with the charm expectation within errors, but clearly requires further statistics to demonstrate a signal. PHENIX has many handles on the production of heavy quarks, and the first results are via the measurement of single electrons.

5. Charm via Single Electrons

The measurement of open charm and open beauty in heavy ion collisions is sensitive to the initial gluon densities in the incoming nuclear wavefunctions and possible thermal contributions from later gluon-gluon scattering. In addition, total charm production is a crucial comparison by which to gauge the possible suppression of J/ψ in deconfined matter. Total charm production (integrated over all transverse momentum) may be expected to be suppressed relative to binary scaling due to shadowing of the gluon parton distribution in nuclei or enhanced due to thermal production in later stages. Also, it was first predicted that high transverse momentum charm quarks will lose energy in a dense gluonic medium, and then later postulated that this energy loss is tempered by the “dead-cone” effect that suppresses co-linear gluon emission for $v \ll c$ partons [10]. Also, if the charm mesons appear in medium they may undergo hadronic interactions.

Electrons resulting from semi-leptonic decays of charm D mesons ($D \rightarrow e + K + \nu$) and beauty B mesons ($B \rightarrow e + D + \nu$) have significant contributions to inclusive measured electrons above 1.0 and 2.5 GeV, respectively. The dominant sources of “background” electrons are from neutral pion Dalitz decay ($\pi^0 \rightarrow \gamma e^+ e^-$) and photon conversions in material in the PHENIX aperture. We can account for these sources using our measured π^0 distributions. In addition, although their contributions are relatively small, we must model additional electrons from $\eta, \eta', \omega, \phi, \rho$.

We have published [7] our results from Run I Au-Au collisions at $\sqrt{s_{NN}} = 130 \text{ GeV}$ and find a significant excess of electrons over “background” above $p_T \approx 0.7 \text{ GeV}/c$ that

increases with p_T . The lower data points in Figure 6 are the minimum bias transverse momentum distribution of non-photonic electrons. The results are consistent within relatively large errors with a PYTHIA 6.152 [8] charm calculation using CTEQ5L parton distribution functions and assuming that charm scales with the number of binary collisions.

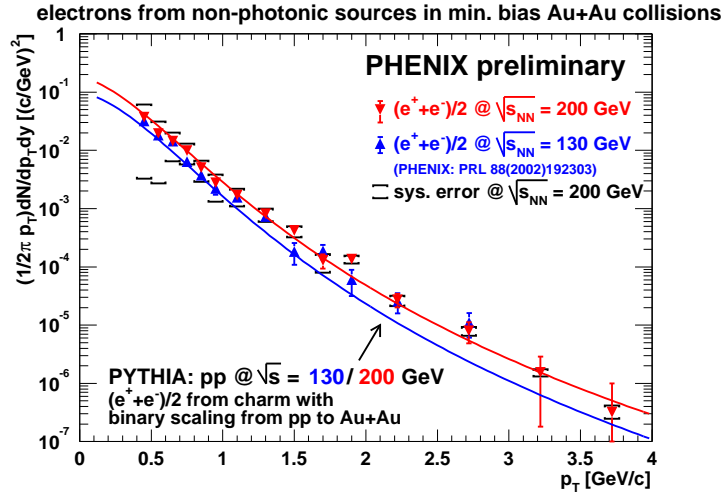


Figure 6. Invariant transverse momentum distribution of electrons from non-photonic sources in “minimum bias” Au-Au collisions compared with expectations from PYTHIA for semi-leptonic charm D meson decay.

The production mechanism within PYTHIA is dominantly the fusion of gluons to produce a $c\bar{c}$ pair. The charm quark then fragments into a D meson which can decay semi-leptonically yielding an electron. However, an alternative picture is that the charm quarks re-scatter in the medium and take part in hydrodynamic expansion. We have used PHENIX derived hydrodynamic model parameters from our measured pion, kaon and proton data, and calculated the shape of the D meson distribution. After simulating the D meson decays, we find equally good agreement with our Run I single electron transverse momentum shape.

In Run II, we have a more powerful method of extracting the single electron charm contribution. Most of the “background” sources are photonic in origin. Thus, in Run II we had a special set of runs with a brass photon converter wrapped around the beam pipe near the interaction point. This material increases by a fixed factor the number of electrons whose source is photonic. Since there is a fixed relation between the γ from π^0 decay (which is the dominant source of conversion photons), and the Dalitz contribution $\pi^0 \rightarrow \gamma e^+ e^-$, we can subtract out both contributions. This method has many advantages over the previously described “cocktail” subtraction method, and has completely independent systematic errors. Also, this method subtracts out any direct

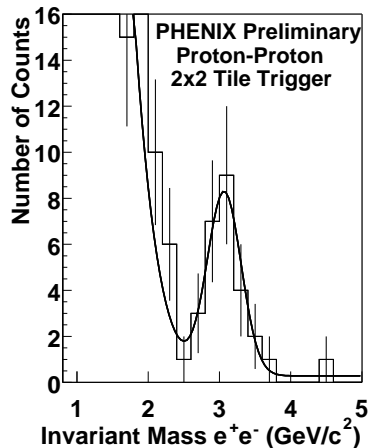


Figure 7. Dielectron invariant mass distribution from proton-proton events where at least one 2x2 EMC tile is above our Level-1 trigger threshold.

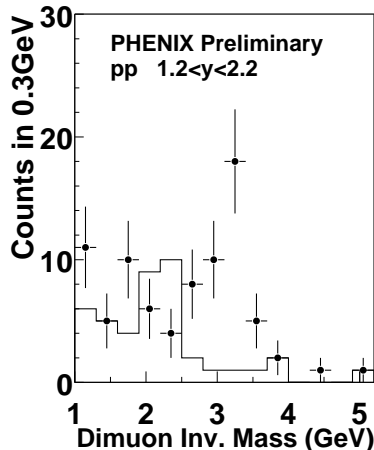


Figure 8. Dimuon invariant mass distribution (points), with unlike sign pair background (histogram) from proton-proton events that fired the Muon Identifier Level-1 dimuon trigger.

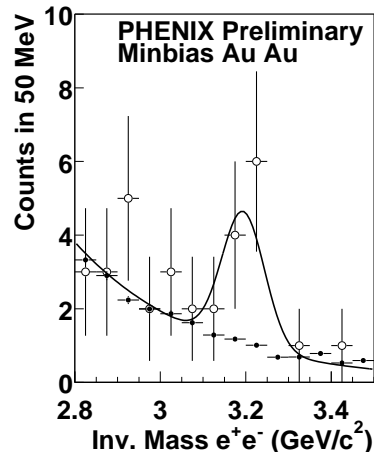


Figure 9. Invariant mass e^+e^- distribution for "minimum bias" (0-90% central) Au-Au collisions at $\sqrt{s_{NN}} = 200$ GeV. Also shown is the mixed event background distribution.

photon contribution to conversion electrons, while the "cocktail" method does not.

After subtraction of the photonic contributions, we show as the upper points in Figure 6 the minimum bias transverse momentum distribution of non-photonic electrons. Again, the data appear reasonably described by a PYTHIA calculation of the expected charm contribution assuming binary collision scaling. The electron data in four centrality bins appear to qualitatively follow binary collision scaling as described in [9]. Significant work remains to reduce the systematic errors in order to exactly quantify this scaling relation. PHENIX is currently analyzing the proton-proton data set so that we can calculate the charm scaling without relying on the PYTHIA baseline.

At this point, we can make the following qualitative observations. (1) Our electron data are consistent with charm expectations and binary scaling within our current statistical and systematic errors. (2) The NA50 experiment at the CERN-SPS has observed an enhancement in intermediate mass dimuons [11]. One possible interpretation is a factor of three enhancement of charm in central Pb-Pb collisions relative to proton-proton. We do not see such an effect at RHIC energies. (3) PHENIX reports a substantial suppression in high transverse momentum π^0 relative to binary scaling [12]. We do not see such a large suppression in the single electrons from charm. This could be due to a lower charm quark energy loss in the dense gluonic medium due to the "dead-cone" effect. Further quantification of these observations is forthcoming.

6. J/ψ Physics

We expect a screening of the QCD attractive potential as we approach the deconfinement transition. The color screening may result in a decrease in the production of heavy quarkonia (J/ψ , ψ' , Υ , etc.) [13]. Alternatively, there are models that predict an enhancement of heavy quarkonia due to $c\bar{c}$ coalescence as the collision volume cools [15]. This enhancement has a large dependence on the total charm production.

6.1. Proton-Proton Results

We present here the first measurements of J/ψ production in proton-proton collisions at $\sqrt{s} = 200$ GeV. We show in Figure 7 the dielectron invariant mass distribution for proton-proton collisions with at least one 2x2 calorimeter tower tile above our Level-1 trigger threshold. This represents about half of our proton-proton statistics, some of which are from additional 4x4 calorimeter tower tile Level-1 triggers. We show in Figure 8 the dimuon invariant mass distribution for proton-proton collisions.

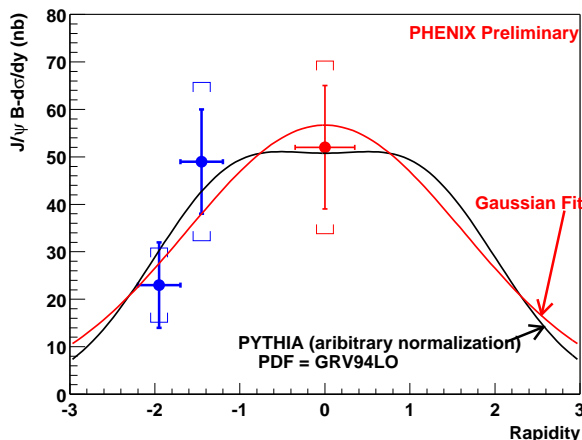


Figure 10. $B_{ll} d\sigma/dy$ as a function of rapidity for $pp \rightarrow J/\psi + X$.

We have corrected for the central and muon arm acceptances, tracking and particle identification efficiencies, and Level-1 trigger efficiencies. We show in Figure 10 the J/ψ branching fraction to leptons (B) times $d\sigma/dy$ as a function of rapidity. The central rapidity point is from our dielectron measurement and the muon data is divided into two rapidity bins. The data are fit to a simple Gaussian form and also to the predicted rapidity shape from PYTHIA using parton distribution function GRV94LO. Removing the branching fraction and integrating over rapidity, we find:

$$\sigma(pp \rightarrow J/\psi + X) = 3.8 \pm 0.6(\text{stat}) \pm 1.3(\text{sys}) \mu\text{b} \quad [\text{PRELIMINARY}] \quad (5)$$

6.2. Gold-Gold Results

Shown in Figure 9 is the dielectron invariant mass distribution for “minimum bias” (0-90% central) Au-Au collisions, along with a mixed event distribution. Further details are in [17]. Although the statistics are limited, we have calculated $B_{ee} dN/dy|_{y=0}$ in three Au-Au centrality ranges, where B_{ee} is the J/ψ branching fraction to electrons. The ranges correspond to 0-20%, 20-40%, and 40-90% central with calculated average number of binary collisions of 791, 297, and 45, respectively. We show the $B_{ee} dN/dy|_{y=0}$ per binary collision as a function of the collision centrality (represented by the number of calculated participating nucleons) in Figure 11. Note that we have also included our midrapidity J/ψ measurement in proton-proton collisions with one binary collision. The statistical errors are shown as lines and the systematic errors as brackets.

On the same figure, we show different possible models of the J/ψ centrality dependence. All the models have been arbitrarily normalized to perfectly intersect the center of our proton-proton data point. This graphical presentation can be somewhat misleading since it effectively assumes no error on the proton-proton measurement. However, we can perform an unbiased measure of agreement using a statistical confidence level. The statistical confidence level is defined as the probability, based on a set of measurements, that the actual probability of an event is better than some specified level. We find that the statistical confidence level is 16%, 80%, and 75% for (1) a model assuming binary collision scaling of the J/ψ , (2) a model assuming binary collision scaling followed by “normal” nuclear absorption with a 7.1 mb cross section, and (3) the exact pattern of suppression relative to binary scaling observed by the NA50 experiment at lower energies [16], respectively. It is notable that although the binary collision scaling model is statistically less favorable, all three models have acceptable confidence levels without consideration of our current systematic errors. Also, we hope to measure the “normal” nuclear absorption in deuteron-nucleus reactions at RHIC in the next two years.

There are two extreme models of J/ψ production at RHIC. One is a simple extrapolation from models used to describe the lower energy NA50 results that imply that almost all $c\bar{c}$ correlations are broken up and one should have over an order of magnitude more suppression [14]. Another is that although all initial J/ψ are destroyed, they are recreated via coalescence of uncorrelated $c\bar{c}$ in the late stages of the time evolution. This mechanism can lead to an enhancement of J/ψ relative to binary collisions (which is statistically less likely given our data).

With the data set from Run II, we can expect a factor of two more statistics from our Level-2 dielectron triggered data in Au-Au, in addition to results at forward rapidity from our dimuon measurements. Also, we are now confident in our abilities to trigger at high RHIC luminosity, and eagerly await a larger data set.

7. Summary

In summary, the PHENIX program of leptonic observables has started with data from Run II. We have the first observation of J/ψ at $\sqrt{s_{NN}} = 200$ GeV in both proton-proton and Au-Au systems. We have shown results on ϕ production, dielectron continuum, and single electrons from charm D meson decay. We have shown just the tip of the iceberg of the PHENIX leptonic observables, and are excited about prospects for future high

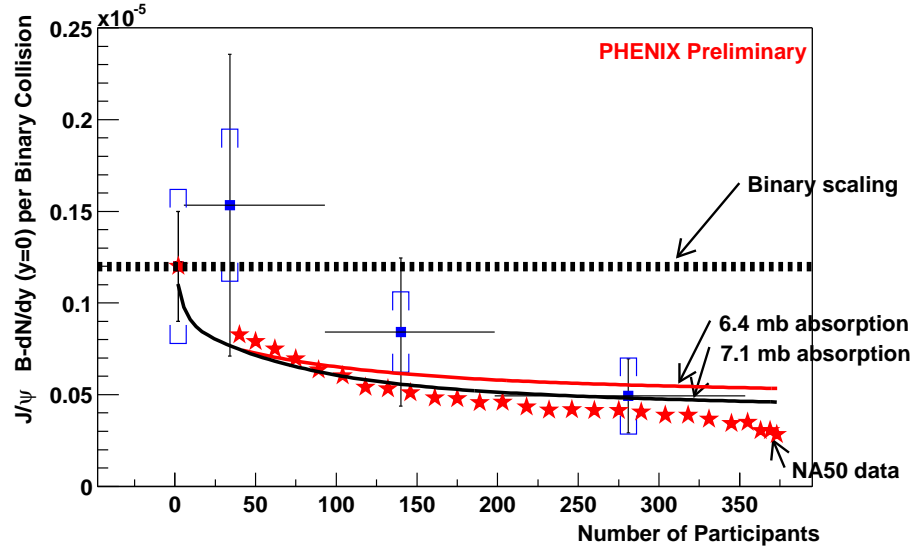


Figure 11. J/ψ branching fraction to electrons times dN/dy at midrapidity ($y=0$) as a function of collision centrality (Number of Participants). The yields are per calculated binary collision. Shown are both the PHENIX proton-proton and Au-Au data points.

luminosity running at RHIC.

REFERENCES

1. PHENIX Collaboration, Nucl. Inst. Meth. to be submitted.
2. V. Koch, Int. J. Mod. Phys. E6, 203 (1997).
3. S. Johnson *et al.* Eur.Phys.J. C18, 645-649 (2001).
4. D. Mukhopadhyay *et al.* (PHENIX Collaboration), these proceedings.
5. E. Yamamoto *et al.* (STAR Collaboration), these proceedings.
6. R. Rapp and J. Wambach, Adv. Nucl. Phys. 25, 1 (2000).
7. K. Adcox *et al.* (PHENIX Collaboration), Phys. Rev. Lett. 88, 192303 (2002).
8. T. Sjostrand *et al.* (PYTHIA), Comput. Phys. Commun. 135, 238 (2001).
9. R. Averbeck *et al.* (PHENIX Collaboration), these proceedings.
10. Y.L. Dokshitzer and D.E. Kharzeev, Phys. Lett. B519, 199 (2001).
11. M.C. Abreu *et al.* (NA50 Collaboration), Eur. Phys. Jour. C14, 443 (2000).
12. S. Mioduszewski *et al.* (PHENIX Collaboration), these proceedings.
13. T. Matsui and H. Satz, Phys. Lett. B178, 416 (1986).
14. B. Zhang *et al.*, Phys. Rev. C62, 054905 (2002).
15. R.L. Thews *et al.*, Phys. Rev. C63, 054905 (2001).
16. M.C. Abreu *et al.* (NA50 Collaboration), Phys. Lett. B521, 195 (2001).
17. A.D. Frawley *et al.* (PHENIX Collaboration), these proceedings.